Imaging of Lung Function using Hyperpolarized Helium-3 Magnetic Resonance Imaging: Review of Current and Emerging Translational Methods and Applications

Sean Fain, PhD[1], **Mark L. Schiebler, MD**[1], **David G McCormack, MD, FRCPC**[2], and **Grace Parraga, PhD**[2]

[1] Department of Medical Physics, University of Wisconsin-Madison, Madison, WI USA

[2] Imaging Research Laboratories, Robarts Research Institute and Departments of Medical Biophysics, Medical Imaging, Biomedical Engineering, The University of Western Ontario London Canada

Abstract

During the past several years there has been extensive development and application of hyperpolarized helium-3 (HP ^{3}He) magnetic resonance imaging (MRI) in clinical respiratory indications such as asthma, chronic obstructive pulmonary disease, cystic fibrosis, radiation-induced lung injury and transplantation. This review focuses on the state-of-the-art of hyperpolarized ^{3}He MRI and its application to clinical pulmonary research. This is not an overview of the physics of the method, as this topic has been covered previously. We focus here on the potential of this imaging method and its challenges in demonstrating new types of information that has the potential to influence clinical research and decision making in pulmonary medicine. Particular attention is given to functional imaging approaches related to ventilation and diffusion-weighted imaging with applications in chronic obstructive pulmonary disease, cystic fibrosis, asthma and radiation-induced lung injury. The strengths and challenges of the application of ^{3}He MRI in these indications are discussed along with a comparison to established and emerging imaging techniques.

INTRODUCTION

Rationale for functional imaging of the lung

Over the past twenty five years, magnetic resonance (MR) imaging has developed as a critical research and diagnostic tool. This is mainly due to the unique tissue contrast of water and fat protons (^{1}H) in their local tissue environments provided by MRI, but MRI also readily provides relatively high 3D spatial and temporal resolution, especially in comparison to other functional imaging methods such as PET and SPECT ([1]). However, until recently, MR imaging of low proton or ^{1}H, density regions of the lungs have been much more challenging than other body tissues because of the inherently low ^{1}H abundance and corresponding low ^{1}H signal. Furthermore, the multitude of air-tissue interfaces within the

Correspondence: G Parraga PhD, Imaging Research Laboratories, Robarts Research Institute, 100 Perth Drive, London, ON, N6A 5K8. Phone: 519-931-5265, FAX: 604-931-5260, gep@imaging.robarts.ca.

lung also create significant magnetic field distortions, or susceptibility artifacts, which further diminish the lung MR ^{1}H signal. Moreover, respiratory and cardiac motion during image acquisition can further degrade pulmonary MR image quality. While respiratory gating and/or rapid breath-hold imaging methods substantially attenuate the effects of motion, low proton density and susceptibility effects together result in significant technological roadblocks that have hampered the clinical utility and use of pulmonary MRI.

The development of inhaled hyperpolarized (or magnetized) Helium-3 (^{3}He) and Xenon-129 (^{129}Xe) contrast agents overcomes the low proton density issues related to normal and diseased lung tissues. Polarization is most commonly achieved using the spin exchange optical pumping (SEOP) method ([2–4]) although the metastability exchange process can also be used to polarize the ^{3}He nucleus ([5]). Both processes increase nuclear polarization of the unpaired nuclear proton in these atoms of up to five orders of magnitude compared to the modest linear increase with field strength using thermal polarization ([6–9]). This increased nuclear polarization compensates for the low density of inhaled noble gas nuclei within the lung (as compared to the abundance of tissue-based protons) and provides ventilation images of the airways and airspaces of the entire lung. Typically, achievable resolution is 1 mm in plane and 5–10 mm out of plane within a breath-hold interval. Currently ^{3}He MRI is most commonly used in research even though the global quantities of ^{3}He are very limited and expensive ([10]). Volatility in the market cost of ^{3}He (e,g, $600–$1900/Liter in 2009) is partly due to government and political considerations, but the limited supply of this agent will likely have highly restricted reimbursable clinical applications for the foreseeable future. For the other noble gas used in pulmonary imaging, ^{129}Xe, the fractional solubility in the blood stream (~17% at equilibrium ([11])) has additional applications for measuring parameters related to gas exchange. Nonetheless, the application of HP ^{129}Xe MRI has lagged behind HP ^{3}He MRI methods largely because ^{129}Xe is more challenging to polarize ([4]), has a lower gyromagnetic ratio than ^{3}He (11.8 MHz/T vs 32.4 MHz/T) and as well, clinical and research protocols for its application are not as fully developed. Consequently, HP ^{129}Xe MRI in human subjects is only superficially treated in this review, although there have been recent advances in both polarization physics ([12–13]) and application in human studies ([14–15]) that should encourage further translation of this technique given its more favorable cost and availability profile for research and clinical applications.

Several excellent reviews focusing on the MR physics and methodology of imaging with polarized gases are in the literature ([13,16–19]). The principal aim of this review is to focus on clinical and research applications of this imaging technology. In practice using the SEOP method, the ^{3}He gas is polarized over a period of 12–14 (overnight) and inhaled by subjects from a bag mixed with medical nitrogen for immediate breath-hold imaging (8–16s). The method is safe, requires no ionizing radiation dose, and can be repeatedly inhaled facilitating longitudinal ([20–21]), interventional, ([22]) and pediatric ([23]) exams. There is now extensive experience using ^{3}He MRI in human subjects and most typically no respiratory adverse events are reported although mild events in less than 10% of subjects ([24–25]) are not uncommon. These mild adverse events are primarily related to a temporary feeling of lightheadedness and are short lived. Importantly, there is no trend towards increased adverse events in more severe disease, which is significant given that the primary safety concern is due to the anoxic He-Nitrogen gas mixture that replaces the air in the lungs during this test. Even extended breath-holds of 10–20 s rarely result in the measured pulse oxymetry hemoglobin saturation falling below 90% for more than a few seconds ([25]). There are now a number of commonly used measurements derived from HP ^{3}He MRI including the static airway functional measurement of ^{3}He ventilation, the structural measurement of airspaces using the ^{3}He apparent diffusion coefficient (ADC), and the dynamic measurement of ^{3}He gas wash-in and wash-out characteristics. Here we review the important and relevant clinical

research contributions of the ^{3}He MRI measurements of the lung airspaces and airway structure and function for healthy subjects and in lung disease.

Hyperpolarized ^{3}He MRI of Ventilation

Hyperpolarized ^{3}He MRI provides an opportunity to visualize those areas of the lung that participate in ventilation and those that do not. This is particularly true for the terminal respiratory bronchioles and their adjacent alveoli that are only ventilated by diffusion. As shown in Figure 1, in healthy young adults, a single inhalation of hyperpolarized ^{3}He gas results in homogeneous signal suggesting that all areas of the lung are participating equally in ventilation. In contrast, characteristic volumetric "focal" defects are observed in COPD and asthma, corresponding to areas of the lung that are not ventilated or are poorly ventilated within the time-course of a typical 8–16s breath-hold scan. Focal defects [26] are identified as regions with no signal or reduced signal relative to surrounding areas (Figure 1) that often create a pattern of spatially heterogeneity now recognized as a defining characteristic of both COPD [27–28] and asthma [29]. All 3 major lung imaging platforms (CT, MRI, and PET) have documented surprising and large sub-segmental and even segmental ventilation defects in asthmatics [30–32]. For asthma specifically, the extent of heterogeneity revealed by HP ^{3}He MRI is surprising because defects are observed even in asymptomatic patients and appear to involve the central airways, contradicting some conventional assumptions about obstructive lung diseases, previously thought to diffusely involve predominantly small airways with little or no change in the larger airways.

Ventilation defects in healthy normal subjects are relatively common although these defects are typically small (<3 cm) and confined to the peripheral regions of the lungs [33–34]. Consequently there is substantial overlap between normal volunteers, patients with COPD and patients with asthma with respect to the number and size of ventilation defects. Although, on average the lungs of patients with obstructive disease have more numerous and larger defects that become more pronounced as disease becomes more severe [28,33]. While it remains possible that some of these normal subjects have early-onset disease, [28] further study of the reproducibility and sensitivity of ventilation defect measures is required before this can be claimed definitively.

One of the main strengths of MRI using HP noble gases is in their ability to safely evaluate lung function longitudinally without ionizing radiation. This is of particular importance for younger individuals where the risk of cancer induced by medical radiation is thought to be of importance [35]. Important new observations about disease progression and persistence in asthma patients have shown greater than half of defects are persistent over time periods of several days to over a year, [20] further challenging the common perception of asthma as a dynamic disease with highly reversible sites of airway obstruction. A more systematic study found that 75% of defects were reproducible day-to-day and that a similar number did not change in size [21]. Moreover, the persistence of ventilation defects in these studies was observed to be independent of asthma severity and medication use, suggesting that these defects were refractory to therapy. The ultimate clinical significance of these fixed ventilation defects remains unknown and represents an area for further study.

The development of consistent protocols for gas inhalation that control for gas polarization and lung inflation volume are important for consistent interpretation of the clinical meaning of ventilation defect severity and pattern and for quantifying ventilation defect measures. Due to the fact that hyperpolarized noble gases continue to be regulated as unapproved-for-marketing drug contrast agents by national drug agencies, calibration of polarized nuclei concentration in human subject studies has been well controlled to within 1–2% using external low field (~5–10 Gauss) calibration NMR systems. Typical doses are in the 5ml/kg subject weight range, however, in recent studies, the volume of He/N_2 mixture used is

individually adjusted to the subject's total lung capacity to normalize the inflation volume across subjects ([30,36]) to total lung capacity (TLC). Novel approaches to investigate the effects of inflation volume, compare results before and after respiratory maneuvers, such as forced expiration(s) ([37]) and deep inspiration(s) ([22]), that can readily be performed safely in conjunction with bronchodilation or other challenge interventions.

Ultimately, quantitative measures of ventilation and its spatial distribution are critical to the advance of HP noble gas MRI. The most common metric used in the early literature was the mean number of ventilation defects per slice (VDS). While this and similar scores are simple to implement and well suited to consensus evaluation in blinded studies ([33]), they typically condense the defect pattern into a single, whole lung metric, that does not capture regional information about the size and regional distribution of defects. Another approach is to sum the total defect volume observed in the lungs and normalize to total lung volume. In this way, focal ^{3}He ventilation defects can be detected and directly quantified as the ^{3}He MRI ventilation defect volume (VDV) or as a percent ventilation volume (PVV) ([38]). Van Beek and co-workers showed that PVV was significantly different between healthy volunteers, healthy asymptomatic smokers and subjects with COPD, which clearly shows the regional sensitivity of PVV to disease ([39]). In stage III COPD, ^{3}He MRI VDV was also shown to be sensitive to small functional changes over short periods of time ([40]).

More quantitative regional measurement of defect volume better facilitates cross-modality comparisons to abnormalities observed using MDCT and bronchoscopy. These quantitative approaches normalize defect volume to both total lung volume and individual lung lobes, to account for both defect size and distribution ([27,30]). In cases of repeated studies, these measures can be normalized to baseline signal values to calculate fractional ventilated volume ([22]) Alternatively, a spatial coefficient of variation, or standard deviation kernel, can be used to measure signal heterogeneity regionally ([22]). This heterogeneity measure has been used effectively to measure persistence of ventilation defects after deep inspiration in subjects with asthma compared to normal volunteers after methacholine challenge ([22]). Importantly, when ^{3}He MR ventilation images of a patient with stage 3 COPD are directly compared with CT, (Figure 2), there is no anatomical or tissue heterogeneity detected in the CT images that would be predictive of the functional ventalatory changes clearly revealed by HP ^{3}He MRI.

^{3}He MRI Diffusion-weighted imaging

^{3}He is a low density gas with a corresponding high free diffusion constant (~2 cm^2/s) that is biologically inert and effectively insoluble in blood and tissues ([11,41]). Physical diffusion of the gas atoms due to random Brownian motion (as opposed to transmembrane gas diffusion) within the open airspaces of the lung parenchyma can be measured using similar diffusion-weighted imaging (DWI) to that used in DWI of water in conventional MRI ([42]). DWI of ^{3}He gas provides a sensitive and rapid approach for evaluating the lung microstructures generally, including dimensions of the alveoli and acini that define the boundaries of the fundamental units for gas exchange ([43]).

Fick's law predicts that the mean displacement of the gas spins (ℓ) measured over some time interval, (Δ), is approximated by the standard deviation of a Gaussian function given by

$$\ell \approx \sqrt{2\Delta D},(^{44})$$

[1]

When ^{3}He gas is restricted by tissue boundaries, the diffusivity, D, is referred to as the apparent diffusion coefficient, ADC. Typically the diffusion weighting gradients for ^{3}He

MRI applications are short bipolar pulses for which the timing variable, Δ, represents the separation between the diffusion encoding gradient pulses is on the order of 1–2 ms. These short bipolar gradient pulses minimize the TE and breath-hold. For Δ's of 1–2 milliseconds, the average displacement of helium atoms is the same order of magnitude as alveolar diameters (a few hundred micrometers) and this so-called "short range ADC" measure is the one most widely used in patient studies.

In practice, at least two measurements are generally required; one with diffusion encoding gradients applied, S, and one without, S_o. A simple monoexponential model is used to obtain the ADC, where

$$ADC = \frac{1}{b} \ln\left(\frac{S_o}{S}\right).$$

[2]

The ADC image can be interrogated on a pixel-by-pixel basis to provide a quantitative ADC map of surrogate airspace size measurements and accordingly of emphysematous damage ([9,45]). Parametric images of regional ADC changes in the lung are consistent with alveolar changes expected with increases in lung volume, ([36]) gravity dependence, ([36,46]) age ([47]) and etiology of emphysema, i.e. COPD or alph1-antitrypsin ([28,48–49]). Previous COPD studies have shown that ADC correlates with pulmonary function ([46,48,50]) and histological measurements of lung surface area ([51]) and is highly reproducible in COPD ([36]) and sensitive to subclinical disease ([52]) and potentially disease progression ([49]). Values for [3]He ADC range from 0.8 cm^2/s for unrestricted free space (akin to an infinitely large container) to 0.66 cm2/s for an elderly COPD patient (FEV1 26% predicted) and 0.16 cm2/s for a young nonsmoker (FEV1 130% predicted) as shown in Figure 3. Although the free diffusion of [129]Xe is much smaller ([53]) (0.06 vs. 1.8 cm2/s), recent advances in Xe-129 polarization ([12]) have encouraged pre-clinical studies ([54–56]) and several promising pilot studies in human subjects, including diffusion weighted imaging to obtain measures of short range ADC in the lungs of healthy normal subjects (Figure 4), support the extension of DWI with [129]Xe.

An important limitation of ADC is that it represents a relative measure that does not directly represent a quantitative structural dimension that can be related to a measure on histology, for example. The ADC measured on different platforms with different b-values and timing characteristics will necessarily yield different absolute values ([57]). This has motivated efforts to relate diffusion values to measureable histological features such as mean length and surface area to volume. In the short diffusion time regime, between 1 and 1.6 ms, workers ([51,58–59]) have exploited the known geometry of the pulmonary acinus, as first described by Weibel and coworkers, ([60]) to derive geometric parameters such as mean airspace chord length and surface area to volume ratio and related these to histology measurements in *ex vivo* human lungs.

Long Range Diffusion

Novel approaches have also been used to measure diffusion of HP [3]He in the long time regime, where Δ is on the order of 0.5 to several seconds which would normally be difficult to acquire in the lungs due to the short T2* and limited breath-hold. However, measures of long range diffusion across multiple acini and airways have been achieved by storing the polarization along the longitudinal axis for extended times of 1–1.5 seconds followed by readout of a stimulated echo ([61]). Another approach for measuring long range diffusion uses low spatial frequency (wavelengths 2–3 cm) sinusoidal spin tags applied during breath-hold

and followed by serial images to monitor the tag decay due to depolarization and diffusion ([62]).

Long range diffusion has enabled the exploration of communication and collateral ventilation within healthy and diseased ([63–64]). Initial results have found that long-range ADC is more sensitive to changes associated with COPD and asthma (Figure 5) than short-range ADC, ([62,65–66]) probably reflecting the fact that airway level changes are more pronounced in asthma. Much more restricted diffusion across acinar and airway branches might be expected and, in fact, long range ADC is about 2 orders of magnitude smaller than short range ADC (e.g. 0.002 cm2/s vs. 0.16 cm2/s in healthy lungs). Simulations in generalized branching models predict even smaller long range ADC than is measured ([63]) leading to speculation that collateral ventilation in the healthy lungs is higher than previously thought. However, simulations using more complete models have found predictions more in agreement with measured results ([67–68]) inspiring ongoing debate in the literature.[69]

Dynamic imaging

Breath-hold images are limited to a binary interpretation, i.e. presence or absence, of a ventilation defect. Fast MRI techniques provide the potential for visualizing gas distribution over the full respiratory cycle. Fast MRI acquisitions for dynamic imaging typically employ non-Cartesian k-space trajectories including spiral and radial acquisition with SPGR sequences ([70–71]). Early work in COPD made use of interleaved spiral k-space acquisition to depict delayed flow-in and washout in a single coronal slice followed by extension of this approach to a multi-slice stack of spirals acquisition ([70]). More recently, under-sampled radial MRI methods ([37,71–72]) and stack of spiral acquisition with parallel reconstruction along the slice dimension have been introduced that can provide 3D images at ~1 s temporal resolutions.

Studies of dynamic inhalation and forced exhalation in human subjects have demonstrated spatial and temporal heterogeneity in the uptake and the washout of the HP ^{3}He in asthma (Figure 6) ([37,72]) and CF ([73]). Dynamic methods can also provide quantitative measures, such as arrival time, time to peak and washout slope in regions with partial obstruction that demonstrate diminished but finite gas uptake and/or delayed filling (Figure 7) ([39]). Moreover, dynamic imaging of respiratory dynamics with whole lung coverage may be the only way to assess regional lung function in very sick and pediatric patients.

Mechanical Deformation Studies

Changes in the mechanical properties of the lungs are associated with a variety of restrictive ([74]) and obstructive lung diseases ([75]). Finite element analysis can be used in conjunction with these dynamic images using proton or hyperpolarized gas MRI to calculate regional stress and strain in healthy and diseased lungs. Moreover, these images can be acquired during spirometry maneuvers to further quantify regional lung stiffness and compliance in the context of whole lung function ([76–78]). However, mapping of lung elements over the multiple steps/time frames of the experiment is challenging and represents a serious limitation of conventional MRI is the relative absence of anatomic markers within the lungs. Spin tagging of hyperpolarized gases is an alternative for tracking lung compliance ([79–81]). Recent development of approaches for faster spin tagging sequences have improved temporal resolution, allowing more precise regional depiction of lung deformation during dynamic maneuvers ([82]). More work in this area is required in order to definitively relate these MRI-derived mechanical properties of the lung to established markers of airways disease and interstitial fibrosis. Heretofore, lung compliance has not been measured non-invasively *in vivo*. These new measures of lung structure may provide a fertile area for

further research in the large number of restrictive lung diseases and their progression, or after therapy.

Emerging Approaches

Oxygen-weighted HP gas MRI was one of the earliest methods proposed and demonstrated in animal models ([83]). The gas dose is mixed with pure O_2 immediately prior to inhalation to approximate normoxic concentrations (20% O_2). The T1 decay of ^{3}He and Xe-129 in normoxic mixtures (20% O_2) are on the order of 30 s or greater for field strengths from 1.5–3 T. There is effectively no signal recovery and the T1 signal decay for HP gases is dominated by Radio Frequency (RF)-saturation and the paramagnetic effects of residual oxygen in the lungs ([83]). Consequently, the paramagnetic effects of O_2 that effectively decrease T1 of the polarized gas provide a quantitative estimate of the PO_2 ([83–85]) that can potentially be used to calculate V_A/Q ([86]). Typically, the same slice is imaged at multiple phases and at different delay times to separate RF-saturation of signal from signal loss due to PO_2 concentration ([86]). Recent work has allowed measurement within a single breath-hold ([85,87]). The technique has potential application in pulmonary embolism ([88]) and in bronchiolitis obliterans after lung transplant ([89])

Airway Measurement

All of the aforementioned techniques and most of the previously published techniques focus on the parenchymal space in the lung rather than the large airways. Quantitative measures of airway lumen on multidetector CT (MDCT) ([90]) have shown changes in diseases such as asthma ([91]). However, significant ionizing radiation is associated with MDCT imaging of the lung spaces limiting its use for serial longitudinal and pediatric studies.

Several techniques using ^{3}He MRI have evaluated early-filling time points from dynamic MRI ([92–93]) to isolate the large airways for quantitative measurement of the lumen. Direct measurement of the lumen ([92,94]) or after region growing segmentation of the airway tree ([93]), can be employed. These methods agree well with quantitative CT measures in phantom studies and in human subjects and may provide an alternative to CT for airway lumen measurement in longitudinal and pediatric studies.

Image Guided Interventions

The spatial resolution of ^{3}He MR images is an advantage for guiding the assessment or therapy of heterogeneous diseases of the lungs. For example, bronchoalveolar lavage at ventilation defect sites on HP ^{3}He MRI show that neutrophil cell counts increase with extent of ventilation defect in asthma ([30]). A proposed example of treatment planning using ^{3}He MRI includes recent use of ^{3}He ventilation images to guide so-called "dose painting" in radiotherapy treatment planning ([95–98]). Response to therapy, including radiation-induced lung injury or inflammation (RILI) ([99]) can also be monitored. Similar applications of ^{3}He MRI may increasingly be used to guide interventions as stent placement in COPD ([100]) and smooth muscle ablation treatments in asthma ([101]).

DISCUSSION

It is important to note that ^{3}He MRI is unique among pulmonary imaging methods because of its high spatial and temporal resolution of respiratory disease morphology (ADC) ***and*** function (ventilation volumetry) and its safe use across a wide variety of vulnerable pediatric, respiratory compromised and elderly patients ([25]) to explore mechanisms of disease pathophysiology. Hence, a number of important respiratory diseases have been evaluated in some depth and breadth across different research sites including COPD, asthma, cystic fibrosis and RILI. As with other functional imaging methods that are yet in

the "imaging physics" and "image processing" domain, there remain significant challenges to translating ^{3}He MRI to clinical research and clinical care. The unique ability to measure disease morphological and functional consequences and explore mechanisms of disease pathophysiology does not necessarily directly translate to improved care unless alternative therapies exist that can benefit from the information provided by HP He MRI. However, for the specific cases of asthma and COPD, there is an increasing recognition that different phenotypes exist ([40,102–103]) and that these patient groups may have differential response to therapy. Moreover as therapies become more diverse and patient-specific, imaging with HP He MRI will likely be one of the only ways to verify response and efficacy for an individual patient or group of patients. Nonetheless, HP He MRI techniques need to become more quantitative, sensitive and accessible to justify its current cost and complexity.

As with many functional imaging methods, there remain significant challenges to translating these methods to the clinic. It is also equally important to point out that currently respiratory diseases still have significant unmet treatment needs in terms of pharmaceutical and minimally invasive interventions; and these disorders stand alone among the leading causes of death and disease. As the world becomes more industrialized and polluted, respiratory illnesses will continue to increase in prevalence, morbidity and overall mortality. We believe this is largely the case because up until recently, lung imaging methods have been mainly restricted to x-ray based methods and the lung is particularly radiation sensitive which diminishes the numbers and types of imaging sessions that are practical. While pulmonary function testing is quite reliable and inexpensive there are many diseases that can not be easily diagnosed by this type of functional lung testing. Imaging is often not used in the diagnosis of COPD, CF, asthma or RILI in part because unlike many organ systems where early or sensitive diagnosis has lead to earlier and efficacious treatments, there is no such virtuous cycle in place for most respiratory diseases. As shown in Table 1, these current and emerging imaging methods for respiratory disease each have significant strengths and challenges. It is in this context or clinical reality that we continue to vigorously support the research and development of ^{3}He MRI methods even in light of the increased costs, decreased availability and access that are predicted for the near future.

Acknowledgments

References

1. Vidal Melo MF, Layfield D, Harris RS, et al. Quantification of regional ventilation-perfusion ratios with PET. J Nucl Med. 2003; 44:1982–1991. [PubMed: 14660725]

2. Bouchiat M, Carver T, Varnum C. Nuclear polarization in ^{3}He gas induced by optical pumping and dipolar exchange. Phys Rev Lett. 1960; 5:373–375.

3. Happer W, Miron E, Schaefer S, Schreiber D, Vanwijngaarden WA, Zeng X. Polarization of the Nuclear Spins of Noble-Gas Atoms by Spin Exchange with Optically Pumped Alkali-Metal Atoms. Physical Review A. :3092–3110.

4. Walker TG, Happer W. Spin-exchange optical pumping of noble-gas nuclei. Reviews of Modern Physics. 1997; 69:629–642.

5. Colegrove F. Polarization of He-3 gas by optical pumping. Physical Review. 1963; 132:2561.

6. Albert MS, Cates GD, Driehuys B, et al. Biological magnetic resonance imaging using laser-polarized ^{129}Xe. Nature. 1994; 370:199–201. [PubMed: 8028666]

7. Middleton H, Black RD, Saam B, et al. MR imaging with hyperpolarized 3He gas. Magn Reson Med. 1995; 33:271–275. [PubMed: 7707920]

8. MacFall JR, Charles HC, Black RD, et al. Human lung air spaces: potential for MR imaging with hyperpolarized He-3. Radiology. 1996; 200:553–558. [PubMed: 8685356]

9. Kauczor HU, Ebert M, Kreitner KF, et al. Imaging of the lungs using 3He MRI: preliminary clinical experience in 18 patients with and without lung disease. J Magn Reson Imaging. 1997; 7:538–543. [PubMed: 9170039]

10. Cho A. Physics. Helium-3 shortage could put freeze on low-temperature research. Science. 2009; 326:778–779. [PubMed: 19892947]

11. MacDonald, A.; Wann, K. Physiological Aspects of Anaesthetics and Inert Gases. London: Academic Press; 1978.

12. Ruset IC, Ketel S, Hersman FW. Optical pumping system design for large production of hyperpolarized Xe-129. Physical Review Letters. 2006:96.

13. Hersman FW, Ruset IC, Ketel S, et al. Large production system for hyperpolarized Xe-129 for human lung imaging studies. Academic Radiology. 2008; 15:683–692. [PubMed: 18486005]

14. Patz S, Muradian I, Hrovat MI, et al. Human pulmonary imaging and spectroscopy with hyperpolarized Xe-129 at 0.2T. Academic Radiology. 2008; 15:713–727. [PubMed: 18486008]

15. Patz S, Hersman FW, Muradian I, et al. Hyperpolarized Xe-129 MRI: A viable functional lung imaging modality? European Journal of Radiology. 2007; 64:335–344. [PubMed: 17890035]

16. Moller HE, Chen XJ, Saam B, et al. MRI of the lungs using hyperpolarized noble gases. Magn Reson Med. 2002; 47:1029–1051. [PubMed: 12111949]

17. van Beek EJ, Wild JM, Kauczor HU, Schreiber W, Mugler JP 3rd, de Lange EE. Functional MRI of the lung using hyperpolarized 3-helium gas. J Magn Reson Imaging. 2004; 20:540–554. [PubMed: 15390146]

18. Fain SB, Korosec FR, Holmes JH, O'Halloran R, Sorkness RL, Grist TM. Functional lung imaging using hyperpolarized gas MRI. J Magn Reson Imaging. 2007; 25:910–923. [PubMed: 17410561]

19. Emami K, Stephen M, Kadlecek S, Cadman RV, Ishii M, Rizi RR. Quantitative assessment of lung using hyperpolarized magnetic resonance imaging. Proc Am Thorac Soc. 2009; 6:431–438. [PubMed: 19687215]

20. de Lange EE, Altes TA, Patrie JT, et al. The variability of regional airflow obstruction within the lungs of patients with asthma: assessment with hyperpolarized helium-3 magnetic resonance imaging. J Allergy Clin Immunol. 2007; 119:1072–1078. [PubMed: 17353032]

21. de Lange EE, Altes TA, Patrie JT, et al. Changes in regional airflow obstruction over time in the lungs of patients with asthma: evaluation with ^{3}He MR imaging. Radiology. 2009; 250:567–575. [PubMed: 19188325]

22. Tzeng YS, Lutchen K, Albert M. The difference in ventilation heterogeneity between asthmatic and healthy subjects quantified using hyperpolarized ^{3}He MRI. J Appl Physiol. 2009; 106:813–822. [PubMed: 19023025]

23. Altes TA, de Lange EE. Applications of hyperpolarized helium-3 gas magnetic resonance imaging in pediatric lung disease. Top Magn Reson Imaging. 2003; 14:231–236. [PubMed: 12973130]

24. Altes, TA.; Gersbach, JC.; Mata, JF.; JPM; Brookeman, JR.; deLange, EE. Evaluation of the safety of hyperpolarized helium-3 gas as an inhaled contrast agent for MRI. Proc Intl Soc Mag Reson Med 15; Seattle, WA. 2007. p. 1305

25. Lutey BA, Lefrak SS, Woods JC, et al. Hyperpolarized ^{3}He MR imaging: physiologic monitoring observations and safety considerations in 100 consecutive subjects. Radiology. 2008; 248:655–661. [PubMed: 18641256]

26. Samee S, Altes T, Powers P, et al. Imaging the lungs in asthmatic patients by using hyperpolarized helium-3 magnetic resonance: assessment of response to methacholine and exercise challenge. J Allergy Clin Immunol. 2003; 111:1205–1211. [PubMed: 12789218]

27. Woodhouse N, Wild JM, Paley MN, et al. Combined helium-3/proton magnetic resonance imaging measurement of ventilated lung volumes in smokers compared to never-smokers. J Magn Reson Imaging. 2005; 21:365–369. [PubMed: 15779032]

28. van Beek EJ, Dahmen AM, Stavngaard T, et al. Hyperpolarised 3He MRI versus HRCT in COPD and normal volunteers: PHIL trial. Eur Respir J. 2009; 34:1311–1321. [PubMed: 19541712]

29. Bousquet J, Jeffery PK, Busse WW, Johnson M, Vignola AM. Asthma. From bronchoconstriction to airways inflammation and remodeling. Am J Respir Crit Care Med. 2000; 161:1720–1745. [PubMed: 10806180]

30. Fain SB, Gonzalez-Fernandez G, Peterson ET, et al. Evaluation of Structure-Function Relationships in Asthma using Multidetector CT and Hyperpolarized He-3 MRI. Acad Radiol. 2008; 15:753–762. [PubMed: 18486011]

31. Tgavalekos NT, Tawhai M, Harris RS, et al. Identifying airways responsible for heterogeneous ventilation and mechanical dysfunction in asthma: an image functional modeling approach. J Appl Physiol. 2005; 99:2388–2397. [PubMed: 16081622]

32. Altes TA, Powers PL, Knight-Scott J, et al. Hyperpolarized 3He MR lung ventilation imaging in asthmatics: preliminary findings. J Magn Reson Imaging. 2001; 13:378–384. [PubMed: 11241810]

33. de Lange EE, Altes TA, Patrie JT, et al. Evaluation of asthma with hyperpolarized helium-3 MRI: correlation with clinical severity and spirometry. Chest. 2006; 130:1055–1062. [PubMed: 17035438]

34. Lee EY, Sun Y, Zurakowski D, Hatabu H, Khatwa U, Albert MS. Hyperpolarized ^{3}He MR imaging of the lung: normal range of ventilation defects and PFT correlation in young adults. J Thorac Imaging. 2009; 24:110–114. [PubMed: 19465833]

35. Fazel R, Krumholz HM, Wang Y, et al. Exposure to low-dose ionizing radiation from medical imaging procedures. N Engl J Med. 2009; 361:849–857. [PubMed: 19710483]

36. Diaz S, Casselbrant I, Piitulainen E, et al. Hyperpolarized ^{3}He apparent diffusion coefficient MRI of the lung: reproducibility and volume dependency in healthy volunteers and patients with emphysema. J Magn Reson Imaging. 2008; 27:763–770. [PubMed: 18344208]

37. Holmes JH, O'Halloran RL, Brodsky EK, Jung Y, Block WF, Fain SB. 3D hyperpolarized He-3 MRI of ventilation using a multi-echo projection acquisition. Magn Reson Med. 2008; 59:1062–1071. [PubMed: 18429034]

38. Parraga G, Mathew L, Etemad-Rezai R, McCormack DG, Santyr GE. Hyperpolarized (3)he magnetic resonance imaging of ventilation defects in healthy elderly volunteers initial findings at 3.0 tesla. Acad Radiol. 2008; 15:776–785. [PubMed: 18486013]

39. Koumellis P, van Beek EJ, Woodhouse N, et al. Quantitative analysis of regional airways obstruction using dynamic hyperpolarized ^{3}He MRI-preliminary results in children with cystic fibrosis. J Magn Reson Imaging. 2005; 22:420–426. [PubMed: 16104046]

40. Mathew L, Kirby M, Etemad-Rezai R, Wheatley A, McCormack DG, Parraga G. Hyperpolarized (3)He magnetic resonance imaging: Preliminary evaluation of phenotyping potential in chronic obstructive pulmonary disease. Eur J Radiol. 200910.1016/j.ejrad.2009.10.028

41. Chen X, Moller H, Chawla M, et al. Spatially resolved measurements of hyperpolarized gas properties in the lung in vivo. Part I: Diffusion coefficient. Magn Reson Med. 1999; 42:721–728. [PubMed: 10502761]

42. Basser PJ, Mattiello J, LeBihan D. Estimation of the effective self-diffusion tensor from the NMR spin echo. J Magn Reson B. 1994; 103:247–254. [PubMed: 8019776]

43. Saam B, Yablonskiy D, Kodibagkar V, et al. MR imaging of diffusion of ^{3}He gas in healthy and diseased lungs. Magn Reson Med. 2000; 44:174–179. [PubMed: 10918314]

44. Bear, J. Dynamics of fluids in porous media. Vol. xvii. New York: American Elsevier Pub. Co; 1972. p. 78

45. Brookeman J, Mugler JP 3rd, Knight-Scott J, Munger T, deLange E, Bogorad P. Studies of ^{3}He diffusion coefficient in the human lung: Age-related distribution patterns. Eur J Radiol. 1999; 9:21.

46. Morbach AE, Gast KK, Schmiedeskamp J, et al. Diffusion-weighted MRI of the lung with hyperpolarized helium-3: a study of reproducibility. J Magn Reson Imaging. 2005; 21:765–774. [PubMed: 15906344]

47. Fain SB, Altes TA, Panth SR, et al. Detection of age-dependent changes in healthy adult lungs with diffusion-weighted ^{3}He MRI. Acad Radiol. 2005; 12:1385–1393. [PubMed: 16253850]

48. Salerno M, de Lange EE, Altes TA, Truwit JD, Brookeman JR, Mugler JP 3rd. Emphysema: hyperpolarized helium 3 diffusion MR imaging of the lungs compared with spirometric indexes--initial experience. Radiology. 2002; 222:252–260. [PubMed: 11756734]

49. Diaz S, Casselbrant I, Piitulainen E, et al. Progression of emphysema in a 12-month hyperpolarized 3He-MRI study: lacunarity analysis provided a more sensitive measure than standard ADC analysis. Acad Radiol. 2009; 16:700–707. [PubMed: 19362025]

50. Diaz S, Casselbrant I, Piitulainen E, et al. Validity of apparent diffusion coefficient hyperpolarized ^{3}He-MRI using MSCT and pulmonary function tests as references. Eur J Radiol. 2009; 71:257–263. [PubMed: 18514455]

51. Woods JC, Choong CK, Yablonskiy DA, et al. Hyperpolarized ^{3}He diffusion MRI and histology in pulmonary emphysema. Magn Reson Med. 2006; 56:1293–1300. [PubMed: 17058206]

52. Fain SB, Panth SR, Evans MD, et al. Early emphysematous changes in asymptomatic smokers: detection with ^{3}He MR imaging. Radiology. 2006; 239:875–883. [PubMed: 16714465]

53. Patyal BR, Gao JH, Williams RF, et al. Longitudinal relaxation and diffusion measurements using magnetic resonance signals from laser-hyperpolarized 129Xe nuclei. J Magn Reson. 1997; 126:58–65. [PubMed: 9177796]

54. Ruppert K, Mata JF, Brookeman JR, Hagspiel KD, Mugler JP 3rd. Exploring lung function with hyperpolarized (129)Xe nuclear magnetic resonance. Magn Reson Med. 2004; 51:676–687. [PubMed: 15065239]

55. Mansson S, Wolber J, Driehuys B, Wollmer P, Golman K. Characterization of diffusing capacity and perfusion of the rat lung in a lipopolysaccharide disease model using hyperpolarized ^{129}Xe. Magn Reson Med. 2003; 50:1170–1179. [PubMed: 14648564]

56. Abdeen N, Cross A, Cron G, et al. Measurement of xenon diffusing capacity in the rat lung by hyperpolarized ^{129}Xe MRI and dynamic spectroscopy in a single breath-hold. Magn Reson Med. 2006; 56:255–264. [PubMed: 16767751]

57. Gierada DS, Woods JC, Bierhals AJ, et al. Effects of diffusion time on short-range hyperpolarized (3)He diffusivity measurements in emphysema. J Magn Reson Imaging. 2009; 30:801–808. [PubMed: 19787725]

58. Yablonskiy D, Sukstanskii A, Leawoods J, et al. Quantitative in vivo assessment of lung microstructure at the alveolar level with hyperpolarized ^{3}He diffusion MRI. PNAS. 2002; 99:3111–3116. [PubMed: 11867733]

59. Yablonskiy DA, Sukstanskii AL, Woods JC, et al. Quantification of lung microstructure with hyperpolarized 3He diffusion MRI. J Appl Physiol. 2009; 107:1258–1265. [PubMed: 19661452]

60. Bachofen H, Weibel ER. Morphometric Data and Mechanical Models of Lung Structure. Acta Anat. 1981; 111:10–10.

61. Wang C, Miller GW, Altes TA, de Lange EE, Cates GD Jr, Mugler JP 3rd. Time dependence of ^{3}He diffusion in the human lung: measurement in the long-time regime using stimulated echoes. Magn Reson Med. 2006; 56:296–309. [PubMed: 16791861]

62. Woods JC, Yablonskiy DA, Choong CK, et al. Long-range diffusion of hyperpolarized 3He in explanted normal and emphysematous human lungs via magnetization tagging. J Appl Physiol. 2005; 99:1992–1997. [PubMed: 16024528]

63. Bartel SE, Haywood SE, Woods JC, et al. Role of collateral paths in long-range diffusion in lungs. J Appl Physiol. 2008; 104:1495–1503. [PubMed: 18292298]

64. Conradi MS, Yablonskiy DA, Woods JC, et al. The role of collateral paths in long-range diffusion of ^{3}He in lungs. Acad Radiol. 2008; 15:675–682. [PubMed: 18486004]

65. Wang C, Altes TA, Mugler JP 3rd, et al. Assessment of the lung microstructure in patients with asthma using hyperpolarized ^{3}He diffusion MRI at two time scales: comparison with healthy subjects and patients with COPD. J Magn Reson Imaging. 2008; 28:80–88. [PubMed: 18581381]

66. Wang C, Miller GW, Altes TA, et al. Extending the range of diffusion times for regional measurement of the ^{3}He ADC in human lungs. Magn Reson Med. 2008; 59:673–678. [PubMed: 18306375]

67. Verbanck S, Paiva M. Simulation of the apparent diffusion of helium-3 in the human acinus. J Appl Physiol. 2007; 103:249–254. [PubMed: 17379747]

68. Plotkowiak M, Burrowes K, Wolber J, et al. Relationship between structural changes and hyperpolarized gas magnetic resonance imaging in chronic obstructive pulmonary disease using computational simulations with realistic alveolar geometry. Philos Transact A Math Phys Eng Sci. 2009; 367:2347–2369. [PubMed: 19414459]

69. Verbanck S, Paiva M. Determinants of the long-range apparent diffusion coefficient in the human lung: collateral channels or intra-acinar branching? J Appl Physiol. 2009; 106:1023. author reply 1024. [PubMed: 19244557]

70. Salerno M, Altes TA, Brookeman JR, de Lange EE, Mugler JP 3rd. Dynamic spiral MRI of pulmonary gas flow using hyperpolarized (3)He: preliminary studies in healthy and diseased lungs. Magn Reson Med. 2001; 46:667–677. [PubMed: 11590642]

71. Wild J, Paley M, Kasuboski L, et al. Dynamic radial projection MRI of inhaled hyperpolarized ^{3}He gas. Magn Reson Med. 2003; 49:991–997. [PubMed: 12768575]

72. Holmes JH, O'Halloran RL, Brodsky EK, et al. Three-dimensional imaging of ventilation dynamics in asthmatics using multiecho projection acquisition with constrained reconstruction. Magn Reson Med. 2009; 62:1543–1556. [PubMed: 19785015]

73. McMahon CJ, Dodd JD, Hill C, et al. Hyperpolarized 3helium magnetic resonance ventilation imaging of the lung in cystic fibrosis: comparison with high resolution CT and spirometry. Eur Radiol. 2006; 16:2483–2490. [PubMed: 16871384]

74. Baydur A. Pulmonary physiology in interstitial lung disease: recent developments in diagnostic and prognostic implications. Curr Opin Pulm Med. 1996; 2:370–375. [PubMed: 9363170]

75. Sciurba FC. Physiologic similarities and differences between COPD and asthma. Chest. 2004; 126:117S–124S. discussion 159S–161S. [PubMed: 15302772]

76. Gee J, Sundaram T, Hasegawa I, Uematsu H, Hatabu H. Characterization of regional pulmonary mechanics from serial magnetic resonance imaging data. Acad Radiol. 2003; 10:1147–1152. [PubMed: 14587632]

77. Sundaram TA, Gee JC. Towards a model of lung biomechanics: pulmonary kinematics via registration of serial lung images. Med Image Anal. 2005; 9:524–537. [PubMed: 15896996]

78. Voorhees A, An J, Berger KI, Goldring RM, Chen Q. Magnetic resonance imaging-based spirometry for regional assessment of pulmonary function. Magn Reson Med. 2005; 54:1146–1154. [PubMed: 16217776]

79. Owers-Bradley JR, Fichele S, Bennattayalah A, et al. MR tagging of human lungs using hyperpolarized 3He gas. J Magn Reson Imaging. 2003; 17:142–146. [PubMed: 12500284]

80. Cai J, Altes TA, Miller GW, et al. MR grid-tagging using hyperpolarized helium-3 for regional quantitative assessment of pulmonary biomechanics and ventilation. Magn Reson Med. 2007; 58:373–380. [PubMed: 17654579]

81. Cai J, Miller GW, Altes TA, et al. Direct measurement of lung motion using hyperpolarized helium-3 MR tagging. Int J Radiat Oncol Biol Phys. 2007; 68:650–653. [PubMed: 17445997]

82. Cai J, Sheng K, Benedict SH, et al. Dynamic MRI of grid-tagged hyperpolarized helium-3 for the assessment of lung motion during breathing. Int J Radiat Oncol Biol Phys. 2009; 75:276–284. [PubMed: 19540059]

83. Deninger AJ, Eberle B, Ebert M, et al. Quantification of regional intrapulmonary oxygen partial pressure evolution during apnea by (3)He MRI. J Magn Reson. 1999; 141:207–216. [PubMed: 10579944]

84. Deninger AJ, Eberle B, Bermuth J, et al. Assessment of a single-acquisition imaging sequence for oxygen-sensitive (3)He-MRI. Magn Reson Med. 2002; 47:105–114. [PubMed: 11754449]

85. Fischer MC, Spector ZZ, Ishii M, et al. Single-acquisition sequence for the measurement of oxygen partial pressure by hyperpolarized gas MRI. Magn Reson Med. 2004; 52:766–773. [PubMed: 15389934]

86. Rizi RR, Baumgardner JE, Ishii M, et al. Determination of regional VA/Q by hyperpolarized 3He MRI. Magn Reson Med. 2004; 52:65–72. [PubMed: 15236368]

87. Miller GW, Mugler JP 3rd, Altes TA, et al. A short-breath-hold technique for lung pO2 mapping with ^{3}He MRI. Magn Reson Med. 2010; 63:127–136. [PubMed: 19918891]

88. Jalali A, Ishii M, Edvinsson JM, et al. Detection of simulated pulmonary embolism in a porcine model using hyperpolarized ^{3}He MRI. Magn Reson Med. 2004; 51:291–298. [PubMed: 14755654]

89. Gast KK, Biedermann A, Herweling A, et al. Oxygen-sensitive 3He-MRI in bronchiolitis obliterans after lung transplantation. Eur Radiol. 2008; 18:530–537. [PubMed: 17926041]

90. Saba OI, Hoffman EA, Reinhardt JM. Maximizing quantitative accuracy of lung airway lumen and wall measures obtained from X-ray CT imaging. J Appl Physiol. 2003; 95:1063–1075. [PubMed: 12754180]

91. Aysola RS, Hoffman EA, Gierada D, et al. Airway remodeling measured by multidetector CT is increased in severe asthma and correlates with pathology. Chest. 2008; 134:1183–1191. [PubMed: 18641116]

92. Tzeng YS, Hoffman E, Cook-Granroth J, et al. Comparison of airway diameter measurements from an anthropomorphic airway tree phantom using hyperpolarized ^{3}He MRI and high-resolution computed tomography. Magn Reson Med. 2007; 58:636–642. [PubMed: 17763351]

93. Peterson, E.; Holmes, J.; Fain, S. Airway Measurement in 3D using Dynamic Hyperpolarized He-3 Multi-Echo VIPR. Proceedings 16th Scientific Meeting, International Society for Magnetic Resonance in Medicine; Toronto. 2008. p. 2645

94. Lewis TA, Tzeng YS, McKinstry EL, et al. Quantification of airway diameters and 3D airway tree rendering from dynamic hyperpolarized ^{3}He magnetic resonance imaging. Magn Reson Med. 2005; 53:474–478. [PubMed: 15678546]

95. Ireland RH, Bragg CM, McJury M, et al. Feasibility of image registration and intensity-modulated radiotherapy planning with hyperpolarized helium-3 magnetic resonance imaging for non-small-cell lung cancer. Int J Radiat Oncol Biol Phys. 2007; 68:273–281. [PubMed: 17448880]

96. Ireland RH, Woodhouse N, Hoggard N, et al. An image acquisition and registration strategy for the fusion of hyperpolarized helium-3 MRI and x-ray CT images of the lung. Phys Med Biol. 2008; 53:6055–6063. [PubMed: 18843168]

97. Bates EL, Bragg CM, Wild JM, Hatton MQ, Ireland RH. Functional image-based radiotherapy planning for non-small cell lung cancer: A simulation study. Radiother Oncol. 2009; 93:32–36. [PubMed: 19552978]

98. Hodge CW, Tome WA, Fain SB, Bentzen SM, Mehta MP. On the use of hyperpolarized helium mri for conformal avoidance lung radiotherapy. Med Dosim. 200910.1016/j.meddos.2009.09.004

99. Mathew L, Gaede S, Wheatley A, Etemad-Rezai R, Rodrigues GB, Parraga G. Detection of longitudinal lung structural and functional changes after diagnosis of radiation-induced lung injury using hyperpolarized ^{3}He magnetic resonance imaging. Med Phys. 2010; 37:22–31. [PubMed: 20175462]

100. Snell GI, Holsworth L, Borrill ZL, et al. The potential for bronchoscopic lung volume reduction using bronchial prostheses: a pilot study. Chest. 2003; 124:1073–1080. [PubMed: 12970040]

101. Cox G, Thomson NC, Rubin AS, et al. Asthma control during the year after bronchial thermoplasty. N Engl J Med. 2007; 356:1327–1337. [PubMed: 17392302]

102. Moore WC, Bleecker ER, Curran-Everett D, et al. Characterization of the severe asthma phenotype by the National Heart, Lung, and Blood Institute's Severe Asthma Research Program. J Allergy Clin Immunol. 2007; 119:405–413. [PubMed: 17291857]

103. Coxson HO, Mayo J, Lam S, Santyr G, Parraga G, Sin DD. New and current clinical imaging techniques to study chronic obstructive pulmonary disease. Am J Respir Crit Care Med. 2009; 180:588–597. [PubMed: 19608719]
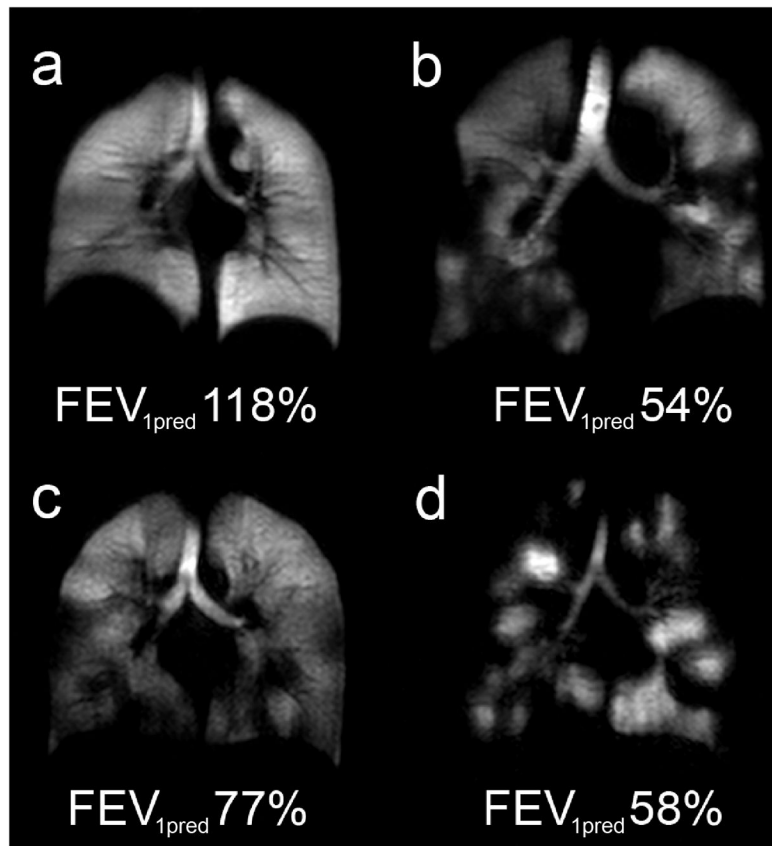
Figure 1. HP He Magnetic Resonance Imaging Static Ventilation Centre Coronal Slice Images
(a) Healthy volunteer 45y female with FEV_1 predicted=118%; (b) Chronic Obstructive Pulmonary Disease 79y male with FEV_1 predicted=54%; (c) Asthma subject at baseline without provocation 26yr male with FEV_1 predicted=77%; (d) Cystic Fibrosis 23y female with FEV_1 predicted=58%.
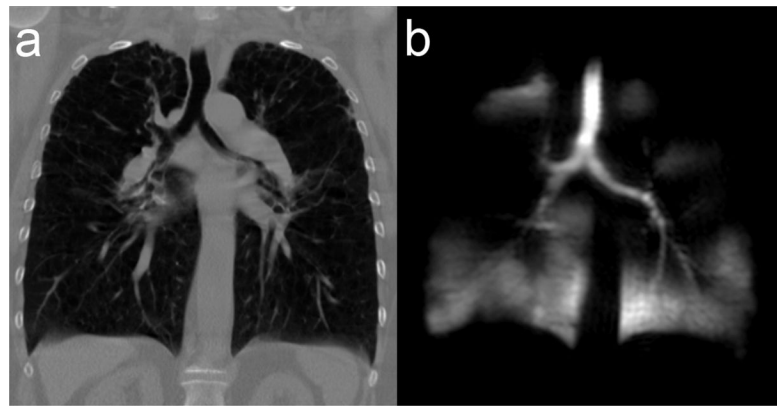
Figure 2. Comparison of high resolution Computed tomography and HP He Magnetic Resonance Imaging in Chronic Obstructive Pulmonary Disease
Female COPD subject 63y with FEV_1 predicted=22%; (a) Centre slice coronal plane reconstruction of high resolution CT; (b) HP He MRI centre coronal slice ventilation image.
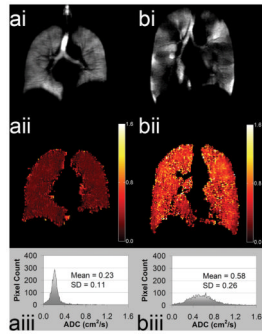
Figure 3. Comparison of HP He Apparent Diffusion Coefficient Maps for Healthy Volunteer and Subject with Chronic Obstructive Pulmonary Disease
(a) Healthy Volunteer male age 58y FEV_1 predicted=108% (i) ventilation (ii) ADC map (iii) ADC histogram. (b) Chronic Obstructive Pulmonary disease male subject age 52y FEV_1 predicted=51% (i) ventilation (ii) ADC map (iii) ADC histogram.
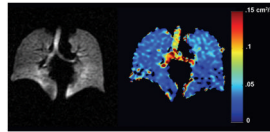
Figure 4.
Spin density and ADC map using single inhalation of HP Xe-129 MRI. The ADC values are much lower due to high density of Xe-129, which may be advantageous in certain diseases for short range diffusion measures. Image courtesy Dr. Bastiaan Driehuys and GE Healthcare.
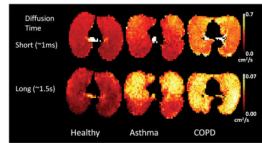
Figure 5.
Comparison of short (top row) and long (bottom row) range diffusion in healthy subject (left) and asthma (middle) and COPD patients (right). Image courtesy Dr. Chengbo Wang, University of Virginia.
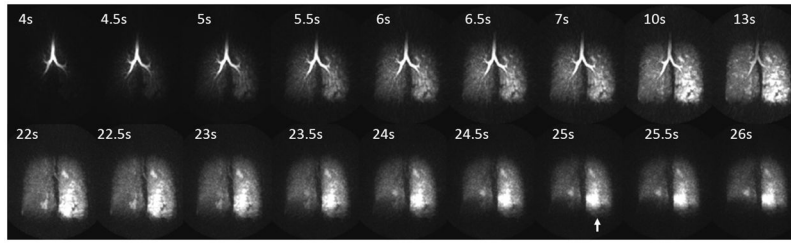
Figure 6.
Coronal maximum intensity projections of a 3D dynamic imaging study using HP ^{3}He-MRI to assess ventilation and gas trapping using a forced exhalation maneuver in asthma. Breath-hold encompasses the time from 10–13s followed by a forced exhalation maneuver showing gas trapping in the left lung most clearly visualized at 25 s (arrow). This patient's FEV_1 was normal, 94% predicted, before and after imaging suggesting significant subclinical heterogeneity and abnormalities of ventilation exist in this patient population.
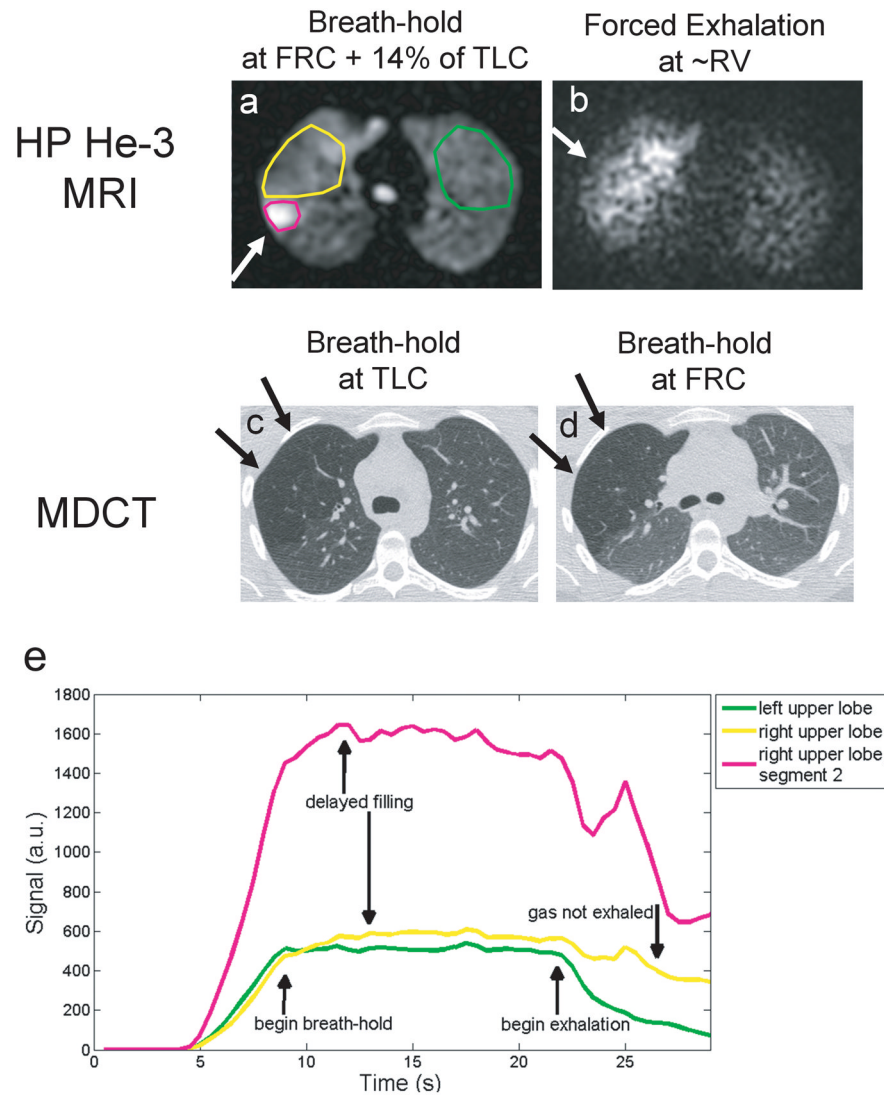
Figure 7.
Results from 3D dynamic MRI in a subclinical finding during inspiration, breath-hold and forced expiration. MRI results in a,b are compared to follow-up MDCT in the same subject in c,d showing hyperlucency in the RUL due to air trapping on MDCT (arrows c,d). Plots of signal time-course for dynamic MRI for the right upper lobe (yellow) compared with left upper lung (green) in the same case. Hyper-intense signal on HP [3]He was found to correspond to the 2nd segment that was not blocked by by a pulmonary aneurysm (green). Note delayed filling as evident by the later time-to-peak signal enhancement relative to the expected trapezoidal shaped enhancement curve in the contra-lateral left lung region.

Table 1

Strengths and Challenges of HRCT and HP ³He MRI for Pulmonary Functional Imaging

	Feasibility		Measurements	Phenotyping	
	Strengths	**Challenges**		**Strengths**	**Challenges**
MDCT	Excellent general availability, cost- effective, easy to implement	Radiation dose requirements for high resolution scans limits longitudinal series and numbers of scans	Mean lung attenuation in HU (LA) Lung attenuation% (LA%) Airway wall area as % of the total size of the airway (WA%)	High spatial resolution	Specialized software required for quantification of airway thickening
HP ³He MRI	Current availability of hardware limited to specialized MR centers; ³He quantities limited globally	Lower spatial resolution than MDCT	Apparent diffusion coefficient (ADC) Ventilation defect volume cm³ (VDV) Ventilation defect score (VDS) Percent ventilated volume (PVV) Ventilation defect volume % (VDV%)	Independent measurements of emphysema and airway occlusion, high sensitivity, excellent precision	Specialized software for quantitative phenotypes, expert observer/ measurement technicians required